JOURNAL OF SPACECRAFT AND ROCKETS
Vol. 31, No. 5, September–October 1994

Hypersonic Rarefied Flow past Spheres Including Wake Structure

Virendra K. Dogra*
ViGYAN, Inc., Hampton, Virginia 23666-0325
and
James N. Moss,† Richard G. Wilmoth,‡ and Joseph M. Price§
NASA Langley Research Center, Hampton, Virginia 23681-0001

Results of a numerical study using the direct simulation Monte Carlo method are presented for hypersonic rarefied flow past spheres. The flow conditions considered are those corresponding to low-density wind-tunnel test conditions. The set of the experimental conditions for the calculations encompasses the transitional to near-continuum flow regimes. Comparison of the calculated drag with experimental results shows good agreement to well within the experimental error. Particular attention is focused on the wake structure. Calculations show that the wake is very rarefied with considerable thermal nonequilibrium for all the cases considered. No flow separation is observed in the wake for the near-continuum case where a vortex has been predicted by Navier-Stokes-type calculations.

Nomenclature

A = frontal area of sphere, $\pi d^2/4$
C_D = drag coefficient, $2D/\rho_\infty V_\infty^2 A$
C_f = skin-friction coefficient, $2\tau_w/\rho_\infty V_\infty^2$
C_p = pressure coefficient, $2p/\rho_\infty V_\infty^2$
D = drag of sphere
d = diameter of sphere
Kn = Knudsen number, λ/d
M = Mach number
$\mathcal{M}$ = molecular weight of air, 28.97 g/mole
$\mathcal{N}$ = Avogadro's number, 6.02252×10^{26} particles/kg-mole
p = pressure
R = gas constant, 287.1 J/kg·K
Re = Reynolds number, $\rho V d/\mu$
Re_2 = total Reynolds number, $\rho V d/\mu_0$
S = speed ratio, $V/\sqrt{2RT}$
s = temperature exponent of the coefficient of viscosity
T = thermodynamic temperature
T_i = internal kinetic temperature
T_{ov} = overall kinetic temperature
T_{rt} = rotational kinetic temperature
T_w = surface temperature
T_t = translational temperature
u = x component of velocity
V = flow velocity
v = y component of velocity
X_i = mole fraction of species i
x = distance from stagnation point measured parallel to freestream
y = distance from symmetry axis measured normal to freestream
Γ = gamma function
γ = ratio of specific heats, 1.4
θ = circumferential angle measured clockwise from stagnation point
λ = mean free path
μ = dynamic viscosity
ρ = density
σ = collision cross section
τ = shear stress

Subscripts

FM = free-molecular-flow values
ith = ith species
0 = stagnation-chamber value
ref = reference value
stag = stagnation point
w = surface values
∞ = freestream values

Introduction

A WIDE range of engineering studies associated with current and projected space vehicles is concerned with the aerothermodynamics of low-density flows. Flows of particular interest can arise from interactions between two or more of the following: the vehicle itself, the wake of the vehicle, the ambient atmosphere, exhaust plumes from upper-stage motors or control motors, and other emitted gas from material outgassing and waste-gas venting. Studies concerned with these interactions are receiving added impetus from the Space Shuttle Orbiter flights, the commitment of several nations to pursue the goal of transatmospheric flight with slender hypersonic vehicles, space experiments, technology demonstration programs such as the Tethered Satellite System 2 (TSS-2), the projected space station, and aeroassisted space transfer vehicles (ASTVs).

Emerging ASTVs will have three primary components: the aerobrake, the payload compartment, and the main propulsion unit. These vehicles will maneuver within the rarefied and generally undefined outer atmosphere rather than just pass through it. Recent studies[1–4] in the transitional flow regime of the aerothermal loads of various blunt bodies associated with current and projected aeroassisted space transfer vehicles have mainly focused on the aerobrake. However, little is known about the wake structure of the aerobrake, which will interact with the payload compartment and main propulsion unit of the vehicle. The heating and aerodynamic forces that can result from the interaction of the near wake with the payload compartment are major concerns, because they can significantly affect the size and the shape of the afterbody configuration. Currently, there is a lack of experimental data on blunt-body wake flows for hypersonic rarefied flows. Recently, the structure of the near wake of the aerobrake in the continuum flow regime has been studied numerically[5] using the Navier-Stokes equations. Although the forebody flow may be in the continuum flow regime, the expansion into the wake region can produce large local Knudsen numbers. Con-

Presented as Paper 92-0495 at the AIAA 30th Aerospace Sciences Meeting, Reno, NV, Jan. 6–9, 1992; received Jan. 23, 1992; revision received Feb. 7, 1994; accepted for publication March 18, 1994.

*Research Engineer. Associate Fellow AIAA.
†Research Engineer. Fellow AIAA.
‡Research Engineer. Senior Member AIAA.
§Research Engineer.

sequently, it becomes imperative that this problem be investigated with an analysis capable of properly modeling the general features of low-density flows. Such a capability exists in the direct simulation Monte Carlo (DSMC) method, which provides a numerical technique applicable to flows ranging from continuum to free-molecule; however, it is normally applied to the more rarefied flow regimes to minimize the computing requirements. Furthermore, the DSMC method permits the accurate simulation of flows with vortices, as demonstrated by the calculations presented in Refs. 6 and 7.

The sphere is a basic blunt shape and has often been the focus of rarefied-flow research by authors[8–12] in the past. Recently, the aerothermodynamics and surface energetics of spheres in rarefied flow have been studied[13,14] using the DSMC method. Most of these investigations have not considered the details of the wake structure. Furthermore, the numerical calculations reported in Ref. 12 for the near wake structure were made using the Navier-Stokes equations. The validity of the Navier-Stokes description decreases as the flow becomes more rarefied; yet, to the authors' knowledge, a computational database does not exist that provides guidance as to when the Navier-Stokes description becomes inappropriate and how it is manifested in terms of flowfield structure and surface quantities. The present study contributes to the database by providing the results of the DSMC simulations.

The purpose of this paper is to examine the basic features of wake flows and to present a comparison of the numerical results with experimental drag measurements of rarefied flow past spheres. In particular, the wake structure and changes in this structure as a function of flow rarefaction are emphasized. Information from basic studies such as this will provide the basis for improving future numerical simulations of specific design configurations.

Computational Method and Boundary Conditions

The DSMC method[15,16] is used for the present calculations. The method and requirements for application of DSMC have been presented in previous publications and are not repeated here.

The computational domain used for the calculations is large enough so that body disturbances do not reach the upstream and side boundaries. Thus, freestream conditions are specified at these boundaries. The flow at the downstream outflow boundary is supersonic, and vacuum conditions are specified. Steady state was assumed when the number of simulated molecules in the flowfield achieved a fixed value within statistical fluctuations. The average number of simulated molecules in a cell was 15 at steady state. The cell dimensions were less than the local mean free path in the forebody as well as in the wake regions.

The molecular collisions are simulated by the variable hard sphere (VHS) molecular model. This model employs the simple hard-sphere angular scattering law so that all directions are equally possible for the postcollision velocity in the center-of-mass frame of reference. However, the collision cross section is a function of the relative energy in the collision. The experimental data used for the present simulations are for low-energy flow conditions where there are no chemical reactions. Therefore, DSMC simulations are performed using a nonreactive gas model for air, while considering only the energy exchange between translational and rotational energy modes. The freestream viscosity and mean free path are evaluated using the VHS collision model with $T_{\text{ref}} = 300$ K, $d_{\text{ref}} = 4.07 \times 10^{-10}$ m, and the temperature exponent s of the viscosity coefficient equal to 0.75.

Sphere Drag Experimental Data

For the present calculations, six low-density wind-tunnel test conditions are selected from Ref. 17, and are summarized in Table 1. Drag measurements on spheres were made at these conditions by Legge and Koppenwallner[17] using a low-density wind tunnel with a 15-deg-half-angle conical nozzle at Aerodynamische Versuchsantalt in Göttingen, Germany. The drag force was measured through the deflection of the sphere model suspended from thin wires. The sphere surface temperature was kept at adiabatic wall conditions. Further details of the test facility and experimental setup can be found in Ref. 17.

Table 1 Test conditions for experiment[a]

Case	Kn_∞	M_∞	p_0, atm	T_0, K	d, mm
1	0.078	11.25	0.25	600	10
2	0.055	12.18	0.50	600	10
3	0.039	11.25	0.25	600	20
4	0.020	12.43	0.75	600	20
5	0.011	12.83	1.50	600	20
6	0.009	12.92	2.00	600	20

[a]Adiabatic wall.

Table 2 Freestream conditions for DSMC calculations

Case	V_∞, m/s	n_∞, 10^{21}/m^3	ρ_∞, 10^{-5} kg/m^3	T_∞, K	Mole fraction X_{O_2}	Mole fraction X_{N_2}
1	1077.0	0.8608	4.1406	22.80	0.2362	0.7638
2	1080.0	1.1736	5.6455	19.56	0.2362	0.7638
3	1077.0	0.8608	4.1406	22.80	0.2362	0.7638
4	1080.8	1.5956	7.6751	18.81	0.2362	0.7638
5	1081.8	2.7369	13.1656	17.69	0.2362	0.7638
6	1082.0	3.5274	16.9680	17.45	0.2362	0.7638

Table 3 Flow parameters and selected results[a]

Case	λ_∞, 10^{-3} m	S_∞	Re_2	$C_{P_{\text{stag}}}$	C_D	$C_{D_{\text{exp}}}$
1	0.784	9.41	15.16	2.04	1.517	1.481
2	0.553	10.19	20.73	1.96	1.412	1.394
3	0.784	9.41	30.33	1.99	1.417	1.392
4	0.403	10.40	56.41	1.84	1.261	1.242
5	0.231	10.74	96.85	1.82	1.189	1.158
6	0.179	10.81	124.90	1.83	1.166	1.127

[a]$T_w = 600$ K.

Freestream and Wall Conditions

The freestream conditions for rarefied flow are difficult to measure experimentally; therefore the freestream conditions given in Table 2 are obtained assuming the isentropic expansion of the air in the wind-tunnel nozzle:

$$\frac{T_0}{T_\infty} = \left(1 + \frac{\gamma - 1}{2} M_\infty^2\right) \tag{1}$$

$$\frac{p_0}{p_\infty} = \left(1 + \frac{\gamma - 1}{2} M_\infty^2\right)^{\gamma/(\gamma-1)} \tag{2}$$

$$\rho_\infty = \frac{p_\infty}{RT_\infty} \tag{3}$$

$$n_\infty = \frac{\rho_\infty}{\mathcal{M}} \mathcal{N} \tag{4}$$

The freestream mean free path is based on the VHS model, using the number density of the major component of the air (i.e., N_2). It is calculated from the relation

$$\lambda_\infty = \frac{(T_\infty / T_{\text{ref}})^\omega}{[\sqrt{2} n_\infty \sigma_{\text{ref}} (2 - \omega)^\omega \Gamma(2 - \omega)]} \tag{5}$$

$$\omega = s - \tfrac{1}{2} \tag{6}$$

The total-Reynolds-number (Re_2) values given in Table 3 are also calculated using the viscosity coefficient based on the VHS model (see Ref. 16).

The gas-surface interaction is assumed to be diffuse with full thermal accommodation. In order to reduce the computational time required to simulate the adiabatic wall condition of the experiments, the surface temperature is assumed to be constant and equal to the stagnation temperature of the flow ($T_0 = 600$ K).

The freestream parameters along with selected results are summarized in Table 3.

Results and Discussion

Although DSMC simulations were performed for six test cases from the experimental investigation of Ref. 17, special attention has been focused on the near wake structure of case 6 to investigate whether or not a stationary vortex exists in the wake. For conditions similar to case 6, the Navier-Stokes calculations of Ref. 12 predict a stationary vortex in the near wake. As discussed later, the present calculations show no evidence of a wake vortex. Furthermore, they show that there is no vortex even at the condition where the freestream density is an order of magnitude higher than that of case 6.

Flowfield Structure

Figures 1 and 2 present the flowfield structure along the stagnation streamline for cases 1 and 6, respectively. For case 1 ($Kn_\infty = 0.078$), the density profile shows that the shock wave is very diffuse. However, for case 6, where $Kn_\infty = 0.009$, the density profile indicates a shock wave that is thick in terms of the total flowfield disturbance.

Figure 1 shows that there is a large amount of thermal nonequilibrium in the shock-wave and shock-layer regions for case 1, as indicated by the fact that the internal temperature is well below the translational temperature. The difference between the translational and internal temperatures in the shock layer decreases as the freestream Knudsen number decreases. Thus, for case 6, where $Kn_\infty = 0.009$, the flow achieves complete thermal equilibrium behind the shock. However, there is still a considerable amount of thermal nonequilibrium within the shock-wave region, as indicated by Fig. 2.

Selected contours of the nondimensional density ρ/ρ_∞, the overall nondimensional kinetic temperature T_{ov}/T_∞, and the Mach number are shown in Figs. 3 and 4 for cases 1 and 6, respectively. The density contours for case 1 ($Kn_\infty = 0.078$) show (Fig. 3a) that the density rises gradually as the flow approaches the sphere, further showing the diffuse nature of the shock wave that is characteristic of highly rarefied flows. The density ratio varies from a maximum of about 5.4 near the stagnation point to less than 0.05 in the wake.

Significant temperature disturbances (Fig. 3b) extend much farther upstream than the density disturbances. The maximum value of nondimensional temperature is 25 and occurs near the stagnation point, whereas the temperature ratio T_w/T_∞ at the surface is 26.31. This small difference indicates that the flow is not in complete thermal equilibrium with the wall even at the stagnation point. The wake is also a highly nonequilibrium region. At this Knudsen number the molecules in the wake are expected to have a bimodal

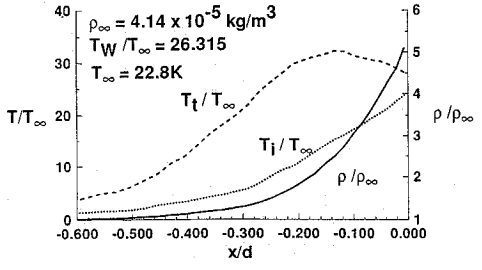

Fig. 1 Flowfield structure along stagnation streamline, case 1: $M_\infty = 11.25$, $Kn_\infty = 0.078$, $T_w = 600$ K, $d = 0.01$ m.

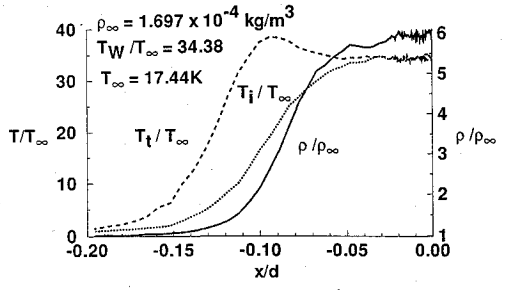

Fig. 2 Flowfield structure along stagnation streamline, case 6: $M_\infty = 12.92$, $Kn_\infty = 0.009$, $T_w = 600$ K, $d = 0.02$ m.

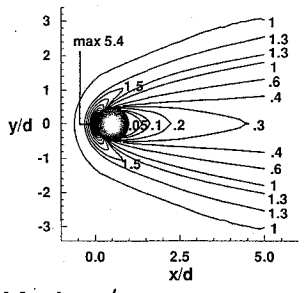

a) Nondimensional density, ρ/ρ_∞

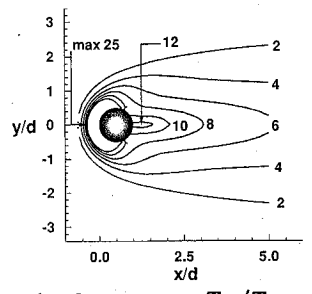

b) Overall nondimensional temperature T_{ov}/T_∞

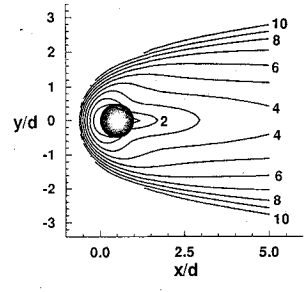

c) Mach number

Fig. 3 Selected contours, case 1: $\rho_\infty = 4.14 \times 10^{-5}$ kg/m^3, $M_\infty = 11.25$, $Kn_\infty = 0.078$, $d = 0.01$ m.

velocity distribution, and therefore the temperatures in the wake are not meaningful in the thermodynamic sense.

The Mach-number contours (Fig. 3c) for case 1 show that the flow decelerates gradually as it approaches the sphere, expands supersonically at the shoulders, and remains supersonic in most of the wake region. For case 6 (Figs. 4a and 4b) the density and temperature contours show a rapid rise of density and temperature as the flow approaches the sphere, further showing the formation of a thick shock wave. Also, the density and temperature disturbances for this case are confined to a smaller region than for case 1. The density ratio varies from a maximum of about 6.27 near the stagnation point to a value of less than 0.05 in the near wake. The Mach-number contours (Fig. 4c) show that the subsonic region in the near wake is considerably larger than that for case 1.

Surface Quantities

The surface-pressure and skin-friction coefficients are presented in Figs. 5a and 5b, respectively. The results are shown as a function of the circumferential angle θ, which is measured clockwise from the stagnation point. The rarefaction effects can be seen by comparing the results for the two cases shown in these figures with those calculated by assuming that case 1 is a free-molecular-flow situation. The variation of pressure coefficient with rarefaction is moderate for the diffuse gas-surface interaction assumed in the present calculations, and all the cases are well below the free-molecule limit. In contrast, the skin friction coefficient is very sensitive to rarefaction, as shown in Fig. 5b. No evidence of recirculation (as would be indicated by negative skin friction) is present.

Sphere Drag

Figure 6 presents a comparison of the calculated drag coefficient with experimental results.[17] This comparison shows that the

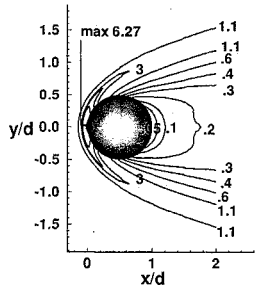

a) Nondimensional density ρ/ρ_∞

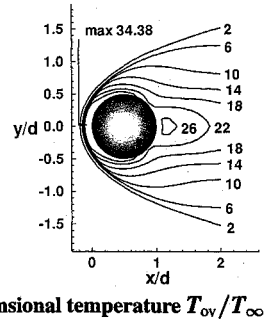

b) Overall nondimensional temperature T_{ov}/T_∞

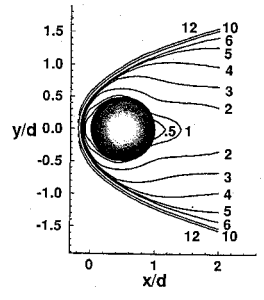

c) Mach number

Fig. 4 Selected contours, case 6: $\rho_\infty = 1.697 \times 10^{-4}$ kg/m^3, $M_\infty = 12.92$, $Kn_\infty = 0.009$, $d = 0.02$ m.

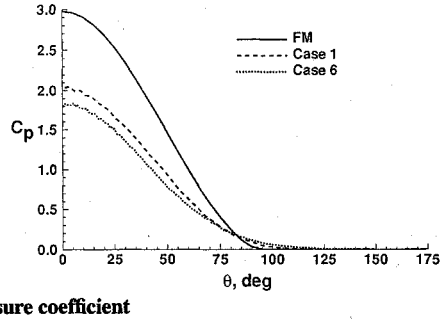

a) Pressure coefficient

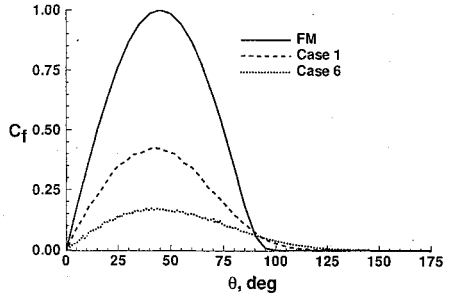

b) Skin-friction coefficient

Fig. 5 Surface quantities.

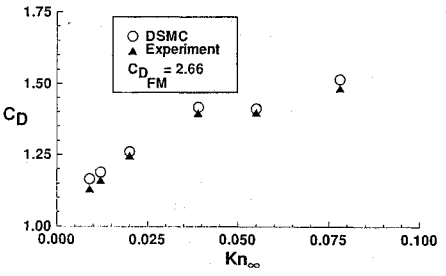

Fig. 6 Sphere drag coefficient.

calculated and experimental values agree to within 4%, which is well within the experimental error. The effect of sphere size on the drag coefficient can be seen by comparing the values in cases 1 and 3 (Table 3), where the freestream conditions are the same for both cases and the sphere diameter for case 3 is twice that of case 1. Both the calculated and the experimental drag coefficient are well below the free-molecule value of 2.66 over this range of Knudsen numbers.

Wake Structure

Under rarefied flow conditions, the flow in the wake of blunt bodies is even more rarefied than the rest of the flowfield. The investigation of the near wake of blunt bodies at these rarefied conditions using the DSMC method generally requires that the entire flowfield be simulated. Because of the large differences in density between the forebody and wake regions, it is difficult to satisfy the usual DSMC computational requirements with regard to number of simulated molecules and time step without exceeding practical computer limits of memory and CPU time. Therefore, a computational approach was used that allowed the wake region to be treated separately, and that approach is described below.

A representative schematic of the computational domain for the DSMC simulations of the complete flowfield of the sphere is shown in Fig. 7a. The number density is generally high in the stagnation region, where very thin cells are required. In order to maintain an appropriate number of simulated molecules in these very thin cells (on the order of 10), the number of real molecules represented by each simulated molecule is set. The thin cells in the stagnation region also require a small time step over which the molecule movement and collision are uncoupled. However, the number density in the wake region of the sphere is very small compared to that in the stagnation region. For a reasonable sample of simulated molecules in the cells of the wake region, each simulated molecule in this region represents a smaller number of real molecules. Since the flux of molecules across region boundaries must also be matched in the DSMC simulations, the time step in the wake region must be reduced to a value that is well below the minimum value required for the forebody calculations. This leads to excessive computational time for simulations.

The above problem has been overcome in the present simulations by performing separate calculations for the wake region with a refined grid and more appropriate time step. The normal component of the flow at the wake-region boundaries is supersonic, and therefore, molecule files are generated (those molecules are registered that cross the boundary to enter the wake) at these boundaries by simulating the entire flowfield domain, where the wake region is not well resolved. Then the wake-region flow is well resolved by performing a secondary DSMC calculation using the previously generated molecule output files as molecule input files at the same boundaries (Fig. 7b). Further details of the general procedure are given in Ref. 18.

The wake portion of the sphere for case 1 is very rarefied and is in a thermal nonequilibrium state. The flow is supersonic even in most of the near wake region (Fig. 3c). The values of temperature in the near wake are characteristic of a bimodal velocity distribution when two streams of molecules move relative to each other. In this case, the molecules from the surface are mixing with the faster molecules coming from the outer region. Figure 8 shows the streamlines for this case. It can be seen that the flow is attached to the sphere surface and there is no evidence of flow separation in the wake, as is

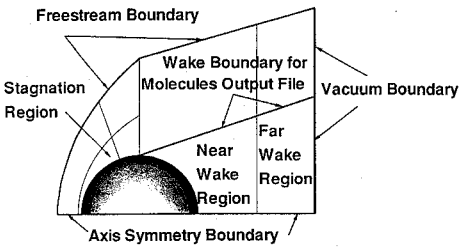

a) Entire flowfield

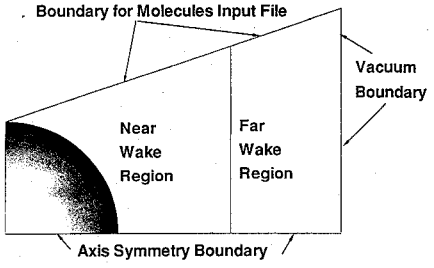

b) Wake flowfield

Fig. 7 Calculation domain and boundaries.

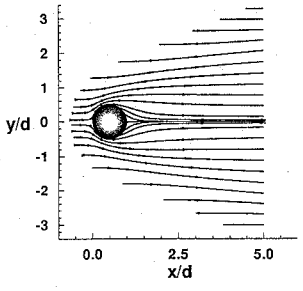

Fig. 8 Streamlines, case 1: $M_\infty = 11.25$, $Kn_\infty = 0.078$, $T_w = 600$ K, $d = 0.01$ m.

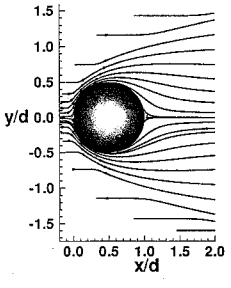

Fig. 9 Streamlines, case 6: $M_\infty = 12.92$, $Kn_\infty = 0.009$, $T_w = 600$ K, $d = 0.02$ m.

expected for this highly rarefied flow condition. A similar pattern of the streamlines is also observed for the other cases.

The experimental flow conditions of case 6 ($Kn_\infty = 0.009$) indicate that the freestream is in the near-continuum flow regime. For similar flow conditions, the sphere wake has been analyzed numerically using the Navier-Stokes equations reported in Ref. 12. For the DSMC simulations, calculations for case 6 are first performed for the entire flowfield including the wake region. Figure 9 shows that there is no indication of flow separation in the wake. In order to obtain further insight into the wake region, a second set of calculations is performed separately for case 6 by the method described above. A very fine grid resolution is used for the cells, so that the dimensions of a cell were less than the local mean free path. Further, a large number of subcells are used to capture even the very small velocity gradient within the cells. The number of molecules stored in the molecule file was close to one-half million, so that statistical error in the wake inflow boundary conditions should be small.

Figure 10 shows the calculated flowfield structure of the wake for case 6. The velocity vectors clearly suggest (Fig. 10a) that there is no evidence of any separation in the wake, whereas the Navier-

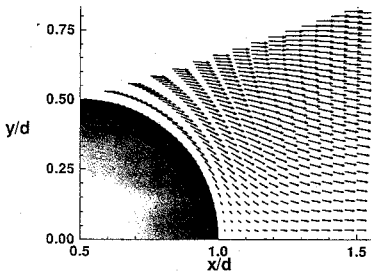

a) Velocity vectors

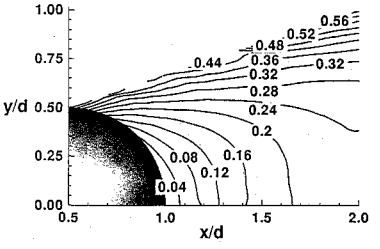

b) Nondimensional density ρ/ρ_∞

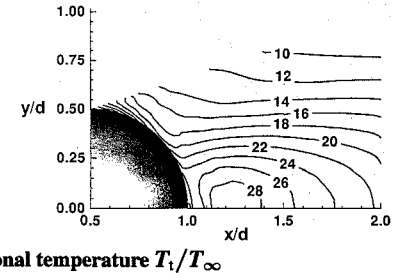

c) Translational temperature T_t/T_∞

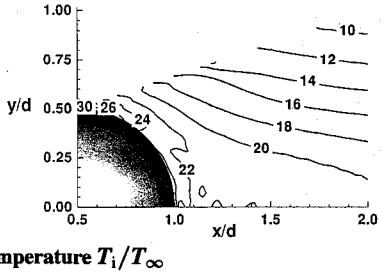

d) Internal temperature T_i/T_∞

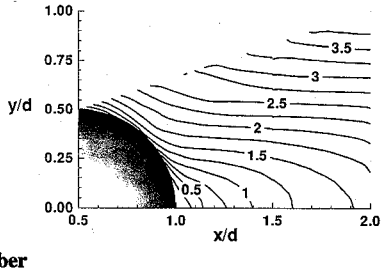

e) Mach number

Fig. 10 Wake flow structure, case 6: $M_\infty = 12.92$, $Kn_\infty = 0.009$, $T_w = 600$ K, $d = 0.02$ m.

Stokes calculations of Ref. 12 have predicted incipient separation with a well-defined recirculation zone. The wake is very rarefied with a considerable amount of thermal nonequilibrium (Figs. 10b, 10c, and 10d). The flow is subsonic in a very small region of the wake (Fig. 10e). Additional calculations were performed to investigate the effect of freestream density, and even with the freestream density an order of magnitude higher than in case 6, a stable vortex is not observed in the wake (Fig. 11). For these higher density calculations the cell dimensions were larger than the local mean free path.

In an attempt to further define the conditions for the onset of a stable separated flow vortex in the wake, the freestream velocity

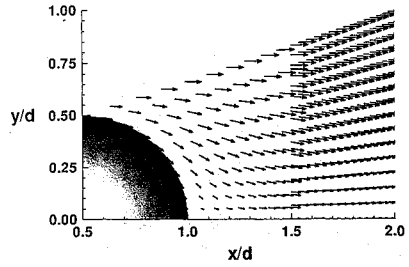

Fig. 11 Wake velocity vectors (vectors not shown for all cells): $M_\infty = 12.9$, $Kn_\infty = 0.0009$, $\rho_\infty = 1.697 \times 10^{-3}$ kg/m^3, $T_w = 600$ K, $d = 0.02$ m.

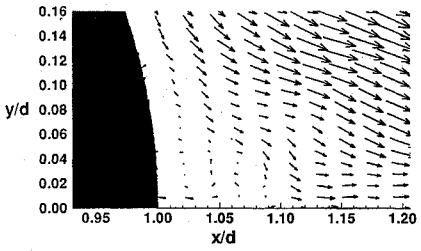

Fig. 12 Wake velocity vectors (magnified view in near wake): $M_\infty = 6.46$, $Kn_\infty = 0.0009$, $\rho_\infty = 1.697 \times 10^{-3}$ kg/m^3, $T_w = 600$ K, $d = 0.02$ m.

was reduced to about half of that for case 6 while maintaining the higher density used for the simulations shown in Fig. 11. The velocity vectors are shown in Fig. 12. These results appear to show a very small (note the scale change) region of highly disorganized flow in the wake. These results were obtained as a time-averaged solution over a large number of time steps after the overall flowfield appeared to have reached the steady state (molecule number settled to a fixed value). However, further studies, possibly using ensembled-averaged unsteady-flow simulations, are needed to determine whether these conditions truly represent incipient separation. Such simulations will obviously impose greater computational demands for the study of transitional wake flows.

The DSMC calculations of Ref. 19 further verify that there is no flow separation for conditions similar to that of case 6, and incipient separation seems to occur at about the same conditions as has been observed in the present study.

Concluding Remarks

DSMC simulations have been performed for a set of six low-density wind-tunnel test conditions. Particular emphasis is placed on the basic features of the sphere wake structure and how the structure changes as a function of flow rarefaction.

The results show that the wake is a rarefied region and there is a large amount of nonequilibrium between translational and internal energy modes for all the cases considered. The calculations also show that there is no flow separation in the wake even for the highest-density case, whereas Navier-Stokes calculations for similar flow conditions have predicted a steady vortex. This discrepancy indicates that the Navier-Stokes formulation becomes inaccurate in the wake, where the flow is very rarefied. Comparison of the calculated sphere drag with experimental results shows agreement to within 4%, which is well within the experimental error. Results of the present study will provide the basis for improving future numerical simulations of the wake flow for specific design configurations.

Acknowledgment

The authors wish to express their appreciation to Dr. G. A. Bird for his assistance in implementing the molecule input output file method as well as for many helpful discussions.

References

[1]Moss, J. N., and Bird, G. A., "Direct Simulations of Transitional Flow for Hypersonic Re-Entry Conditions," *Thermal Design of Aeroassisted Orbital Transfer Vehicles*, edited by H. F. Nelson, Vol. 96, Progress in Astronautics and Aeronautics, AIAA, New York, 1985, pp. 113–139.

[2]Dogra, V. K., Moss, J. N., and Simmonds, A. L., "Direct Simulations of Aerothermal Loads for an Aeroassist Flight Experiment Vehicle," AIAA Paper 87-1546, June 1987.

[3]Celenligil, M. C., Moss, J. N., and Blanchard, R. C., "Three–Dimensional Rarefied Flow Simulations for the Aeroassist Flight Experiment Vehicle," *AIAA Journal*, Vol. 29, No. 1, 1991, pp. 52–57.

[4]Feiereisen, W. J., and McDonald, J. D., "Three Dimensional Discrete Particle Simulation of an AOTV," AIAA Paper 89-1711, June 1989.

[5]Gnoffo, P. A., Price, J. M., and Braun, R. D., "On the Computation of Near Wake, Aerobrake Flowfields," *Journal of Spacecraft and Rockets*, Vol. 29, No. 2, 1992, pp. 182–189.

[6]Bird, G. A., "Direct Simulation of Gas Flows at the Molecular Level," *Communications in Applied Numerical Methods*, Vol. 4, No. 2, 1988, pp. 165–172.

[7]Moss, J. N., Price, J. M., and Chun, C. H., "Hypersonic Rarefied Flow about a Compression Corner—DSMC Simulation and Experiment," AIAA Paper 91-1313, June 1991.

[8]Koppenwaller, G., and Legge, H., "Drag of Bodies in Rarefied Hypersonic Flow," *Thermophysical Aspects of Reentry Flows*, edited by J. N. Moss and C. D. Scott, Vol. 103, Progress in Astronautics and Aeronautics, AIAA, New York, 1986, pp. 44–59.

[9]Kinslow, M., and Potter, J. L., "The Drag of Spheres in Rarefied Hypervelocity Flow," Arnold Engineering Development Center, AEDC-TDR-62-205, Dec. 1962.

[10]Bailey, A. B., "Sphere Drag Measurements in an Aeroballistics Range at High Velocities and Low Reynolds Numbers," Arnold Engineering Development Center, AEDC-TR-66-59, May 1966.

[11]Potter, J. L., and Miller, J. T., "Sphere Drag and Dynamics Simulations in Near-Free-Molecular Flow," *Rarefied Gas Dynamics*, edited by L. Trilling and H. Y. Wachman, Vol. I, Academic Press, New York, 1969, pp. 723–734.

[12]Jain, A. C., and Dahm, W. K., "Hypersonic Merged Layer Blunt Body Flows with Wakes," *Rarefied Gas Dynamics*, edited by Alfred E. Beylich, VCH Weinheim, 1991, pp. 578–587.

[13]Dogra, V. K., Wilmoth, R. G., and Moss, J. N., "Aerothermodynamics of a 1.6-m-Diameter Sphere in Hypersonic Rarefied Flow," *AIAA Journal*, Vol. 30, No. 7, 1992, pp. 1789–1794.

[14]Wilmoth, R. G., Dogra, V. K., and Moss J. N., "Energetics of Gas–Surface Interactions in Transitional Flows at Entry Velocities," *Journal of Spacecraft and Rockets*, Vol. 29, No. 6, 1992, pp. 786–793.

[15]Bird, G. A., *Molecular Gas Dynamics*, Clarendon Press, Oxford, England, UK, 1976.

[16]Bird, G. A., "Monte-Carlo Simulation in Engineering Context," *Rarefied Gas Dynamics*, edited by S. S. Fisher, Vol. 74, Part I, AIAA, New York, 1981, pp. 239–255.

[17]Legge, H., and Koppenwallner, G., "Sphere Drag Measurements in a Free Jet and a Hypersonic Low Density Tunnel," Deutsche Forschungs- und Versuchsanstalt für Luft- und Raumfahrt, E. V., Rept. 70A 37a, Oct. 1970.

[18]Bird, G. A., "The G2/A3 Program System Users Manual," Version 1.6, GAB Consulting Pty Ltd., Sydney, Australia, March 1991.

[19]Brewer, E. B., "Hypersonic Rarefied Wake Characterization," NASA TP-3327, Jan. 1993.